Spatiotemporal extension of extreme heat stress over East Asia under shared socioeconomic pathways

Yujin Kim [a], Seung-Ki Min [a,b,*], Yeon-Hee Kim [a], Eun-Soon Im [c], Dong-Hyun Cha [d], Joong-Bae Ahn [e], Eun-Chul Chang [f], Young-Hwa Byun [g], Youngeun Choi [h]

[a] Division of Environmental Science and Engineering, Pohang University of Science and Technology, Pohang, South Korea
[b] Institute for Convergence Research and Education in Advanced Technology, Yonsei University, Incheon, South Korea
[c] Department of Civil and Environmental Engineering, The Hong Kong University of Science and Technology, Hong Kong SAR, China
[d] School of Urban and Environmental Engineering, Ulsan National Institute of Science and Technology, Ulsan, South Korea
[e] Department of Atmospheric Sciences, Pusan National University, Busan, South Korea
[f] Department of Atmospheric Science, Kongju National University, Gongju, South Korea
[g] Climate Change Research Team, National Institute of Meteorological Sciences, Seogwipo, South Korea
[h] Department of Geography, Konkuk University, Seoul, South Korea

ARTICLE INFO

ABSTRACT

This study examines future changes in extreme heat stress over East Asia and its sub-regions using wet bulb globe temperature (WBGT) based on the CORDEX East Asia Phase II multiple Regional Climate Model (RCM) simulations performed under Shared Socioeconomic Pathways (SSP) scenarios. Daily maximum WBGTs (*WX*) are obtained from 3-hourly bias-corrected WBGTs and their future changes in the late 21st century (2081–2100) are analyzed with respect to the current period (1979–2014). Summer mean *WX* is projected to increase by 3.2 °C (SSP1-2.6: low emission) to 7.6 °C (SSP5-8.5: high emission) over East Asia, dominated by temperature increases. Relative humidity decreases over many regions, slightly offsetting *WX* increases (up to −6%), while it increases in northeastern and northern China, intensifying *WX* increases (up to +14%). This humidity-induced *WX* increase becomes stronger during hottest *WX* days (summer top 5%) and also under low emission scenarios (up to +33%). For sub-regional projections, extreme heat stress day (EHD) is defined when *WX* exceeds its 95th percentile in at least 10% of the area. RCMs project on average a 10 times increase of EHD frequency under the SSP5-8.5 scenario. The EHD magnitude, which combines the intensity and area extent of EHD events, is also expected to increase dramatically throughout East Asia, reaching a range of 3.2–3.5 °C•fraction compared to the current (0.1–0.2 °C•fraction). Further, EHDs are projected to start earlier and end later, lasting much longer (85–140 days) than the current condition (5–6 days) in the SSP5-8.5 scenario. RCMs exhibit a good agreement in *WX* and EHD projections with some noticeable differences in in-land sub-regions. Our results indicate that severe heat stress will affect the whole East Asia throughout and beyond the summer season and, in particular, southern sub-regions will be affected by more-intense and longer-lasting extreme heat stress events.

1. Introduction

The frequency and intensity of extreme heatwaves have increased significantly worldwide since the 1950s, and are projected to become even more frequent and intense in the future, depending on the intensity of global warming (IPCC, 2021). As a result of this intensification of extreme events, there is an expected increase in heat-related illnesses and mortality. In particular, recent studies have projected that severe heatwaves will persistently increase in East Asia (Wang et al., 2019; Ha et al., 2022; Kim et al., 2023), highlighting the need for health-related studies to evaluate the impacts of extreme heat in the region.

The severity of the impacts of extreme heat events increases with higher intensity and longer duration in China (Li et al., 2017). Additionally, the extensive spatial extent of heatwaves can expose a larger population to risks in the United States (Lyon et al., 2019). Moreover, according to Keellings and Moradkhani (2020), as the spatial extent of extreme events increases, their intensity can become stronger and last longer in the United States. Luo et al. (2022) have demonstrated that

---

"continuous spatiotemporal heatwaves," referring to heatwaves that occur in neighboring areas and exhibit spatial continuity while persisting over time, have been expanding in spatial extent and increasing their duration across China since the 1960s, suggesting that understanding the spatiotemporal dynamics of heatwaves is important to describe their temporal and spatial evolution. Kim et al. (2022) have also noted that to quantitatively evaluate the impact of heatwaves on energy demand in South Korea, it is necessary to consider changes in the spatial extent and duration of heatwaves, in addition to their intensity. Therefore, to understand the effects of heatwaves more accurately, it is important to consider the spatial expansion and persistence of heatwaves, in addition to their frequency and intensity. However, there is a lack of research examining these various characteristics of heatwaves at the regional scale.

Furthermore, the impacts of extremely high temperatures on physiology and health can be exacerbated by elevated ambient humidity (Matthews et al., 2017). When high humidity is combined with high temperatures, it can impede the regulation of internal body temperature, thereby increasing the likelihood of heat stroke. Therefore, to evaluate the impact of heatwaves on human health more precisely, both temperature and humidity must be considered (Mora et al., 2017). There are various heat stress indices that incorporate both temperature and humidity. However, these heat stress indices exhibit discrepancies due to the variations in the relative importance of temperature, humidity, and any further quantities in determining heat stress levels. Therefore, it is not feasible to make direct comparisons of the sensitivity of different indices to changes in temperature and humidity on a common scale (Simpson et al., 2023). Therefore, it is essential to select an appropriate index that aligns with the objectives of the analysis.

According to Zamanian et al. (2017), an analysis of the relationship between physiological parameters related to outdoor activities, such as skin temperature, and heat stress indices indicated a strong correlation with indices reflecting relative humidity, like the wet-bulb globe temperature (WBGT) and Humidex. Furthermore, Ioannou et al. (2022) highlighted that WBGT has the highest potential to reflect the physiological strain experienced by workers. The concept of WBGT was first proposed in the 1950s by the US Army and Marine Corps (Yaglou and Minard, 1957), and a simplified WBGT formula that could be calculated using only temperature and relative humidity was devised by the American College of Sports Medicine (ACSM, 1984). Simplified WBGT has the advantage of being easily calculated using only temperature and relative humidity. However, caution is required due to the potential for overestimating heat stress, particularly in hot and humid regions (Chindapol et al., 2017; Kong and Huber, 2022). The simplified WBGT has been utilized in various studies to analyze heat stress (Willett and Sherwood, 2012; Fischer and Knutti, 2013; Im et al., 2017). In a study on East Asia, Liu et al. (2018) predicted that heatwaves defined by WBGT would be more prolonged and severe, particularly in south-eastern China, in the late 21st century, compared to the results using temperature alone. Lee and Min (2018) projected that the spatial extent of extreme heat stress would expand more rapidly in low-latitude regions of East Asia in the late 21st century. When temperature changes are considered together with humidity changes, the areas experiencing severe heat stress are expected to expand faster than those predicted by considering only temperature changes. This result showed the fact that the lower variability of heat stress compared to a single temperature variable leads to a higher signal-to-noise ratio, making it more effective in detecting changes (Fischer and Knutti, 2013; Knutson and Ploshay, 2016). Therefore, it is essential to consider both temperature and humidity to understand the characteristics of heat stress and to assess the impacts of future changes in temperature and humidity on heat stress.

The heat stress is expected to increase globally, but the trend is not the same regionally (Schwingshackl et al., 2021). Also, the heat stress can accompany short-term fluctuations even during a day (Fischer et al., 2012; Takakura et al., 2019), indicating the need for sub-daily temperature and humidity data to obtain the daily maximum heat stress.

Therefore, it is necessary to analyze extreme heat stress in spatial and temporal details for more accurate assessments of its future changes and impacts. Through the Coordinated Regional Domain Experiment (CODEX) East Asia Phase II project, high-resolution (25 km) climate change projection data for the East Asia region has been produced using multiple regional climate models (RCMs) based on the Sixth Assessment Report (AR6) Shared Socioeconomic Pathways (SSP) scenarios. According to Lee et al. (2023), the investigation of the East Asian summer monsoon using a combination of multiple global climate model (GCM)-RCM showed that RCMs simulations better reproduced the duration and extent of the summer monsoon compared to GCMs. This study proved the added value of RCM downscaling in capturing the observed sub-regional characteristics. Additionally, Juzbašić et al. (2022) showed that while the average increase of heat stress intensity in East Asia depends on climate change scenarios, the spatial patterns of heat stress increase are more dependent on the GCM and RCM choices, rather than the scenarios. Therefore, in order to project sub-regional future changes in heat stress and to understand the regional differences in heat stress characteristics, analyses using various RCMs are importantly required. This study projects the future changes in heat stress based on WBGT for East Asia and six sub-regions and evaluates relative contribution of temperature and humidity changes to the heat stress projections. In particular, we examine future changes in characteristics of extreme heat stress events over six East Asian sub-regions considering frequency, intensity, spatial extent, and persistence.

2. Data and methods

2.1. Data

Climate projection data are obtained from the outputs of five RCMs (HadGEM3–RA, CCLM, WRF, RegCM4, and GRIMs) for the domain of 100°–150°E, 20°–50°N. They are the dynamical downscaling products forced by the UK Earth System Model (UK-ESM) Coupled Model Intercomparison Project phase 6 (CMIP6) simulations. The RCMs data used in this study cover both the historical period from 1979 to 2014, as well as the future projection period for the late 21st century (2081–2100), under four different SSP scenarios: SSP1-2.6, SSP2-4.5, SSP3-7.0, and SSP5-8.5 (Table 1). Aiming to perform bias correction using long-term data, we conducted bias correction based on the entire historical simulation period (1979–2014) and analyzed this period as the present climate (see below). Refer to Park et al. (2022) and Juzbašić et al. (2022) for detailed configuration of the RCMs. For WBGT calculation, we used 2 m temperature and relative humidity variables at 3-hour intervals (see below). To ensure consistency, all RCM outputs, with their varying spatial resolutions, were interpolated onto the regular 0.25° × 0.25° latitude-longitude grid of the ERA5 reanalysis (Hersbach et al., 2023). Additionally, five RCMs used different calendar systems. In order to align the temporal coverage, the non-Gregorian RCM data (360 days) were interpolated onto a standard Gregorian calendar. Specifically, days such as 31 Jan, 31 Mar, 31 May, 31 July, 31 Aug, and 31 Dec were generated through interpolation from neighboring days, and days such as 30 Feb (or 29 Feb) were excluded. These processes were conducted before performing the calculations of WBGT. The ERA5 reanalysis data was used to evaluate the performance of the RCMs during the historical period. In addition, this study analyzed heat stress in six sub-regions of East Asia (Fig. 2a), including Northeast China (NEC), North China (NC), Yangtze-Huaihe River Basin (YHR), South China (SC), Korea Peninsula (KP), and Japan (JP).

2.2. Heat stress index

To estimate heat stress, we used the simplified WBGT by ACSM (1984) which is defined as:

$$WBGT = 0.567T_a + 0.393e + 3.94 \tag{1}$$

Table 1

Information of CORDEX East Asia Phase II RCM simulations used in this study.

Driving GCM	RCM	Spatial Resolution	Calendar	Analysis domain and period	
				Spatial	Temporal
UKESM1-0-LL (historical, r1i1p1) in CMIP6 dataset	HadGEM3-RA	$0.22° \times 0.22°$	Gregorian	East Asia: 100-150°E, 20–50°N (land only)	Historical: 1979–2014, 3-hourly
	CCLM	$0.22° \times 0.22°$	360-day		Future:
	WRF	25 km $\times$ 25 km	Gregorian		2081-2100,
	RegCM4	25 km $\times$ 25 km	360-day		3-hourly
	GRIMs	25 km $\times$ 25 km	360-day		

$$e = \left(\frac{RH}{100}\right) \times 6.105 \, exp\left(\frac{17.27 \, T_a}{237.7 + T_a}\right) \qquad (2)$$

where T_a is the air temperature (°C) and e is water vapor pressure (hPa), which is a function of T_a and relative humidity RH (%). The RCMs' 3-hourly temperature and relative humidity data were applied to the WBGT calculation formula, and 3-hourly WBGT values were produced for the historical (1979–2014) and future (2081–2100) periods. In the same way, 3-hourly WBGT data were produced using ERA5 reanalysis data for the period of 1979–2014 and used as a reference dataset for bias correction. Using long-term observational data enables a comprehensive consideration of multiple seasons, years, and climate patterns, leading to a more accurate identification and adjustment of biases within the model. Qiu et al. (2023) showed that among various bias correction methods applied to WBGT based on RCM data, the Quantile Delta Mapping (QDM) preserves the trend of changes and is the most appropriate method for assessing the impact of heat stress. This method aims to correct systematic biases present in climate model simulations by matching the cumulative distribution functions (CDFs) of observed and simulated data for specific variables. In the QDM process, historical climate model data are aligned with corresponding observed data using quantiles. Differences (deltas) between observed and simulated quantiles are calculated and then added to the future model projections to correct for the bias. The QDM is a univariate bias correction method that directly adjusts WBGT and does not consider the inter-variable dependencies between temperature and relative humidity. In this study, the QDM bias correction method was applied to the 3-hourly WBGT data to eliminate the systematic bias in the RCMs. Refer to Qiu et al. (2023) for more details about the QDM bias correction. From bias-corrected 3-hourly WBGTs generated for the historical and future periods, the daily maximum WBGT (defined as *WX*) value was extracted and used in all subsequent analyses.

2.3. Contributions of temperature and humidity to future changes in heat stress

To investigate the drivers of future changes in heat stress over East Asia, we analyzed the respective contributions of temperature (T) and relative humidity (RH). To compare the changes in heat stress between the summer average state and the hottest summer days, the average *WX* from June to August each year was defined as the summer mean *WX* ($\overline{WX}$), and the average *WX* of the hottest summer days that correspond to the top 5% of summer days was defined as $\overline{WX}^*$. We then analyzed the changes in heat stress for both $\overline{WX}$ and $\overline{WX}^*$ and examined the contributions of T and RH to these changes. We obtained *WX* changes

introduced by T under the assumption that RH does not change from its current climatology (i.e. 1979-2014 mean, Table 2). Similarly, *WX* changes due to RH were estimated from using current values of T. Note that we did not separately consider the non-linear interaction term of ΔT and ΔRH, which is addressed as one of the limitations of our study in the conclusion section. For example, we estimated the future changes in *WX* due to T (ΔWX_T) by applying the future T values and current RH values in the *WBGT* formula, and comparing them with the current *WX* values (WX_{cur}). The contributions of T and RH to the changes in *WX* were evaluated by calculating the percentage of the total *WX* change attributable to each factor. The changes in *WX* due to T and RH were converted into percentages of the total *WX* change (Table 2). The resulting percentages represent the proportional contributions (CONT) of T and RH to the overall future change in *WX*. These contributions were calculated for each sub-region. Note that in this analysis, we used the raw T and RH data as well as the raw *WX* without bias correction. When comparing *WX* changes before and after QDM corrections, they show little differences (Fig. S1), indicating that QDM method preserves the trend of future changes as discussed above. Therefore, when analyzing the contributions of T and RH to changes in WX, using the raw data of T, RH, and WX may not introduce a critical problem to reach our conclusion.

2.4. Definition of EHD and related indices for sub-region analysis

First, we defined extreme heat stress day (EHD) as the day when *WX* exceeds the 95th percentile (WX_{95p}) of the summer in the current climate (1979–2014) over an area larger than 10% of the total area within each sub-region. The largest area, NEC, has an approximate coverage of over 140,000 km^2 based on the 10% threshold, while the smallest area, JP, has a spatial extent of 23,700 km^2 as the criterion for defining the spatial extent of EHDs. The threshold for extreme heat stress on each grid is set to the 95th percentile of all *WX* during summer (June–July–August) in the current period. The threshold for extreme was extracted based on the summer, but for the EHD analysis, we extracted EHDs occurring throughout the year (including all months), without restricting to the summer period. Previous studies applied thresholds for spatial extents in extreme events, ranging from 10% to 50% (Peng and Cholaw, 2011; Ren et al., 2012; Wang et al., 2014). In this study, a spatial extent threshold of 10% was applied, which resulted in a similar frequency of EHDs about 10–14 days per year among the six sub-regions in the current climate. Next, to evaluate the impact of extreme events at the regional scale, the frequency (*F*), intensity (*I*), spatial extent (area fraction, *A*), and magnitude (*M*) of EHD were defined (Table 3). Furthermore, the occurrence of extreme heat stress on

Table 2

Calculation method for the contribution (CONT, %) of temperature (T) and relative humidity (RH) to future changes in *WX*. Subscript 'fut' and 'cur' indicate future and current values, respectively.

	Contribution by temperature (T)	Contribution by relative humidity (RH)
Step1	$WX_{Tfut} = 0.567 \, T_{fut} + 0.393e + 3.94 \; e = \left(\frac{RH_{cur}}{100}\right) \times 6.105 \, exp\left(\frac{17.27 \, T_{fut}}{237.7 + T_{fut}}\right)$	$WX_{RHfut} = 0.567 \, T_{cur} + 0.393e + 3.94 \; e = \left(\frac{RH_{fut}}{100}\right) \times 6.105 \, exp\left(\frac{17.27 \, T_{cur}}{237.7 + T_{cur}}\right)$
Step2	$\Delta WX_T = WX_{Tfut} - WX_{cur}$	$\Delta WX_{RH} = WX_{RHfut} - WX_{cur}$
Step3	$CONT_T = (\Delta WX_T / \Delta WX) \times 100$	$CONT_{RH} = (\Delta WX_{RH} / \Delta WX) \times 100$

Table 3

Definition of the common indices in this study.

Component	Definition (Units)
EHD	The day when extreme heat stress ($WX > WX_{95p}$) occurs on 10% or more of the total area of each sub-region
F_{EHD}	The frequency of EHDs (days)
I_{EHD}	The average of intensity, i.e. difference between WX and WX_{95p} over the grids where extreme heat stress occurred (°C)
A_{EHD}	The ratio of the area where extreme heat stress occurred to the total area of sub-region (fraction)
M_{EHD}	The average intensity of EHD weighted by spatial extent, calculated as the multiplied I_{EHD} by A_{EHD} (°C•fraction)
D_{EHD}	The maximum duration of days in which EHD maintained spatial continuity i.e. overlapped by 30% or more (days)
Start and end date	The first and last occurrence dates of the phenomenon where EHD maintains spatial continuity of 30% or more and lasts for at least 3 days during the year.

consecutive days with more than 30% overlap was considered a persistent event (Wang et al., 2018; Yoon et al., 2020), and the duration (*D*) of such events was defined as the number of days from the start date to the end date. For example, as shown in Fig. 1, extreme heat stress occurred in the KP region from August 10 to 19, 2020. On August 10 and 19, the area of extreme heat stress was less than 10% of the total area, so they are not classified into EHD. EHDs occurred continuously for a total of 8 days from August 11 to 18, maintaining spatial coverage overlap more than 30%. On August 11, the EHD affected 25% of the entire KP region, and I_{EHD} was 1.0 °C with M_{EHD} of 0.25 °C•fraction.

3. Results

3.1. East Asian heat stress changes and temperature and humidity contributions

Current climatology in *WX* is first evaluated using multi-model ensemble means (MME) from 5 RCMs. Summer mean *WX* ($\overline{WX}$) is 26.1 °C on average over East Asia, with lower values in high latitudes areas and higher values in low latitudes (Fig. 2a and b). The $\overline{WX}$ of the northernmost NEC region is 24.3 °C, and the YHR and SC regions located at relatively low latitudes are 31.2 °C and 32.5 °C, respectively (Fig. 2a). The 95th percentile of *WX* (WX_{95p}) averaged over East Asia is 30.2 °C, and although there are regional differences, it exceeds the threshold for "high risk (Willett and Sherwood, 2012)" to health (28 °C), leading to the restriction of heavy exercise in all regions (Fig. 2b). In particular, the WX_{95p} in YHR and SC regions are 35.1 °C and 34.9 °C, respectively, far exceeding the threshold (32 °C) of the "extreme risk" level where most outdoor activities are severely constrained. The WX_{95p} value is used as a threshold for EHD analysis for each sub-region (Table 3).

Before examining future changes, the model outputs of RCMs before and after QDM correction were compared with ERA5 reanalysis in terms of climatology (Fig. 2c and d). When the QDM correction method was applied, cold bias from −1.5 to −1.1 °C were corrected depending on RCMs for the summer average (Fig. 2c), and the same correction was found for WX_{95p} from −1.3 to −0.3 °C (Fig. 2d). When comparing the ERA5 with RCMs results after QDM correction, the cold bias of RCMs in both summer mean and extreme threshold were effectively removed, showing very similar results to the observed values for historical period
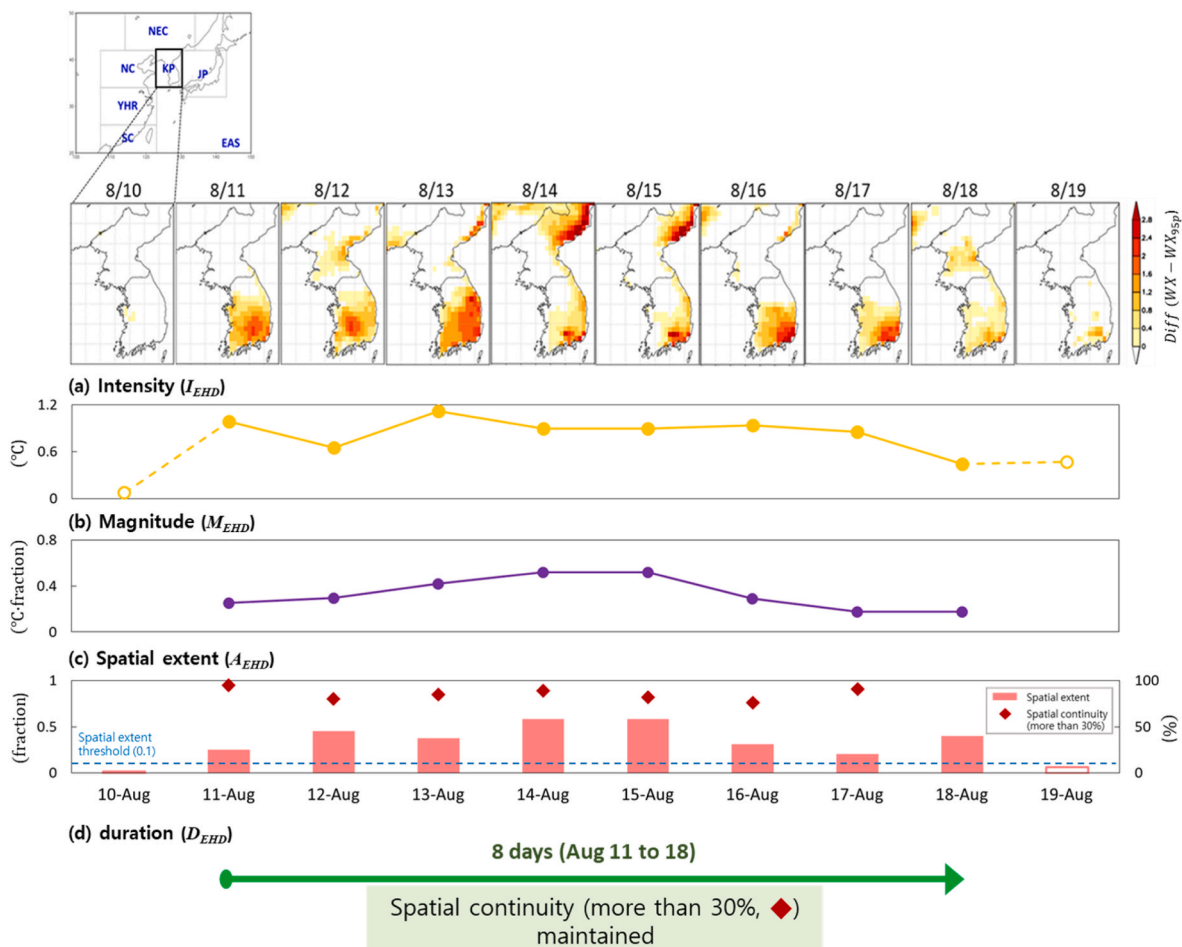

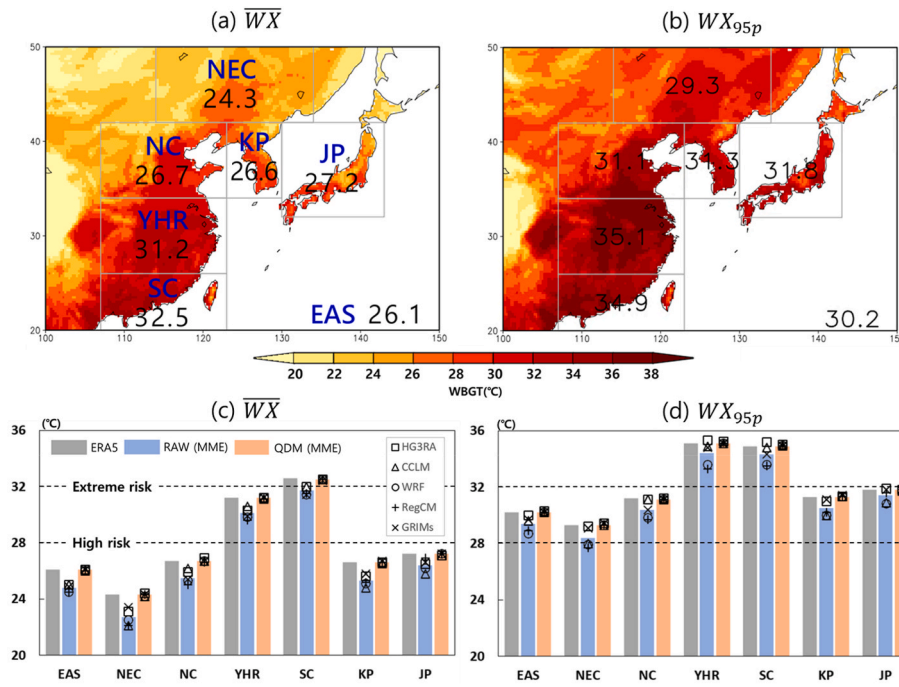**Fig. 1.** An example of EHD events in KP region that lasted from Aug 11 to 18, 2020.

Fig. 2. The spatial distributions of summer (a) mean WX ($\overline{WX}$) and (b) 95th percentile of WX (WX_{95p}) during the current period (1979–2014) from five RCMs MME, and the ERA5 and RCMs values for (c) $\overline{WX}$ and (d) WX_{95p} for each sub-region before and after QDM correction.

(1979–2014).

As global temperatures are projected to rise significantly during the 21st century, leading to increased heat stress worldwide (Coffel et al., 2017), it is anticipated that the increase in summer heat stress will also

be pronounced in the East Asian region. In the late 21st century, the $\overline{WX}$ in East Asia is projected to increase by +3.2 °C in SSP1-2.6 scenario, +4.5 °C in SSP2-4.5 scenario, +6.4 °C in SSP3-7.0 scenario, and +7.6 °C in SSP5-8.5 scenario (Fig. 3a). The higher the emission scenario, the
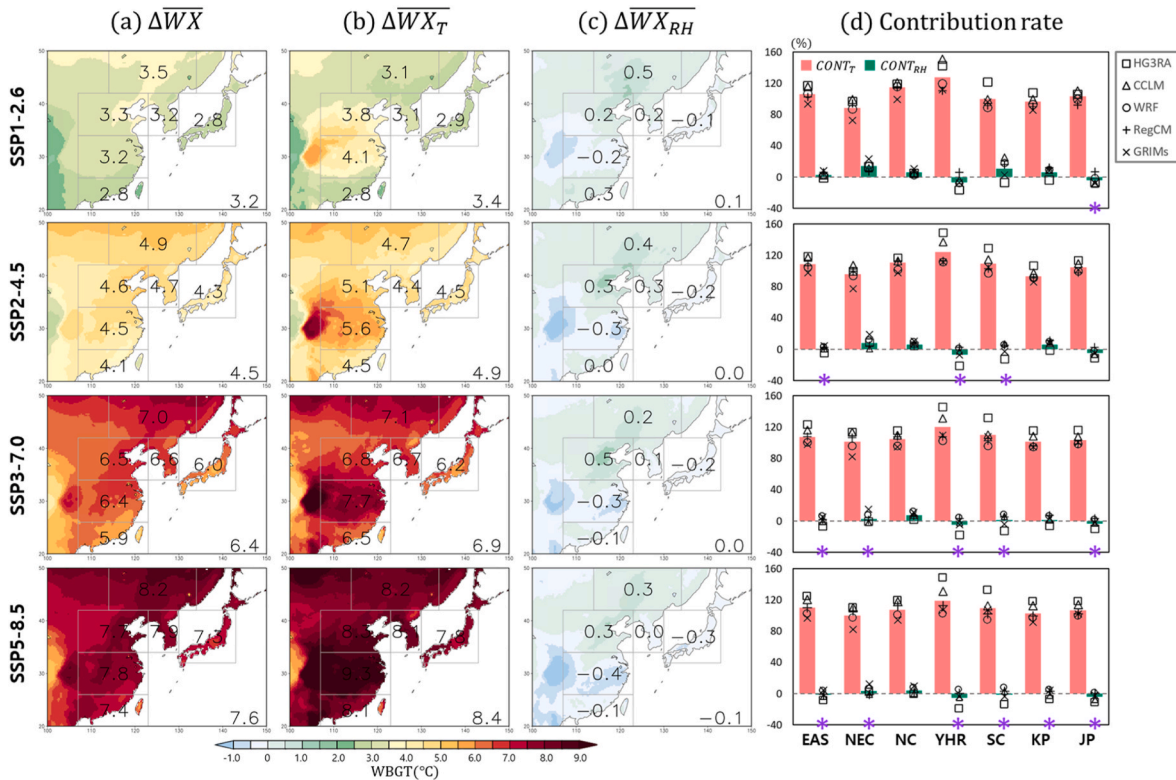

Fig. 3. Spatial distributions of (a) future changes in $\overline{WX}$, (b) changes in $\overline{WX}$ due to changes in temperature (T), and (c) changes in $\overline{WX}$ due to relative humidity (RH) from five RCMs MME, and (d) contribution rate of T and RH to changes in $\overline{WX}$ for East Asia (EAS) and six sub-regions in the late 21st century (2081–2100). (* denote weak consistency among the RCMs, indicating that 3 or fewer models out of 5 RCMs showed a different trend from the MME).

greater the increase. In particular, in the SSP5-8.5 scenario, $\overline{WX}$ in all regions exceeds the 'extreme risk' level (32 °C), indicating that outdoor activities will become difficult during summers in East Asia (Fig. S2). Additionally, the SC region, which currently experiences higher $\overline{WX}$, is expected to have the highest $\overline{WX}$ at 39.8 °C. On the other hand, the NEC region, which is located at high latitudes and has the lowest $\overline{WX}$ among the six regions, currently at 23.4 °C, is projected to have the largest increase in $\overline{WX}$ by +8.2 °C.

The results of the five RCMs show that HadGEM3-RA and GRIMs project a slightly larger increase in $\overline{WX}$ compared to the other models (Fig. S4). When examining the spatial patterns of *WX* changes by RCMs, the CCLM, WRF, and RegCM4 project the greatest increase in high latitude regions and a smaller increase in low latitude regions. However, HadGEM3-RA and GRIMs simulate a larger increase in $\overline{WX}$ in the YHR region as well as in high latitude regions like NEC, and HadGEM3-RA in particular simulates a significant increase in $\overline{WX}$ in SC region compared to the other models. The spatial pattern differences are influenced by the projected future temperatures of each model. While CCLM, WRF, and RegCM4 show the largest temperature increases in NEC, located in the higher latitudes, during the late 21st century, HadGEM3-RA and GRIMs simulations project a greater increase in the YHR compared to the NEC.

The $\overline{WX}$ increases due to the increase in temperature ($\overline{WX_T}$) throughout East Asia, and in most areas, a higher or lower increase is expected when considering relative humidity together (Fig. 3b). In the YHR region, $\overline{WX}$ increases the most significantly due to temperature. The contribution of temperature to the $\overline{WX}$ change is all around 100%, implying that most $\overline{WX}$ changes are explained by temperature (Fig. 3d). On the other hand, the change in $\overline{WX}$ due to relative humidity ($\overline{WX_{RH}}$) varies depending on the region (Fig. 3c). In the NEC and NC regions located in northern China, $\overline{WX}$ increases as relative humidity increases, and the positive contribution of relative humidity is as high as 14%. In

YHR and JP regions, the relative humidity decreases in the future, alleviating the T-induced increase in $\overline{WX}$, showing a negative contribution. According to the SSP scenarios, the effect of relative humidity is greater in the low-emission scenario. In the high-emission scenario, the $\overline{WX}$ increases significantly due to the strong warming, and the contribution of humidity becomes relatively weak. Among the five RCMs, HadGEM3-RA simulates a distinct temperature increase compared to other models (Fig. S6a), indicating a high contribution of temperature and a low contribution of relative humidity. The GRIMs model simulates a significant increase in relative humidity in northern China. Accordingly, the increase of $\overline{WX}$ due to relative humidity is expected to be large in the NEC and NC regions. When considering temperature only, HadGEM3-RA simulated the largest increase in $\overline{WX}$ in all regions (Fig. S6a). However, when considering both temperature and humidity, GRIMs show the strongest increase in $\overline{WX}$ in most regions except the SC (Fig. S3), highlighting differences in model simulations.

It is projected that the hottest summer *WX* ($\overline{WX^*}$), which corresponds to the top 5% *WX* days of summer, will increase by an average of +3.1 °C under the SSP1-2.6 scenario and +7.9 °C under the SSP5-8.5 scenario in East Asia compared to current levels in the late 21st century (Fig. 4). As emission scenarios become more severe, $\overline{WX^*}$ is expected to increase more strongly than $\overline{WX}$. Among the models, GRIMs simulates the strongest increase in $\overline{WX^*}$ (Fig. S5), while RegCM4 project the weakest increase. The changes in $\overline{WX^*}$ due to temperature ($\overline{WX_T^*}$) show an overall increase across East Asia. Except for the NEC, where there is a significant increase in relative humidity, most regions show a higher increase in $\overline{WX_T^*}$ compared to $\overline{WX^*}$ (Fig. 4b). The difference between $\overline{WX^*}$ and $\overline{WX_T^*}$ is smaller than that for the summer mean ($\overline{WX}$). The change in $\overline{WX^*}$ due to relative humidity ($\overline{WX_{RH}^*}$) shows a more distinct regional variation compare to the $\overline{WX}$ (Fig. 4c). The effect of humidity on hottest summer days appears greater than the summer average state (Fig. 4d), inducing
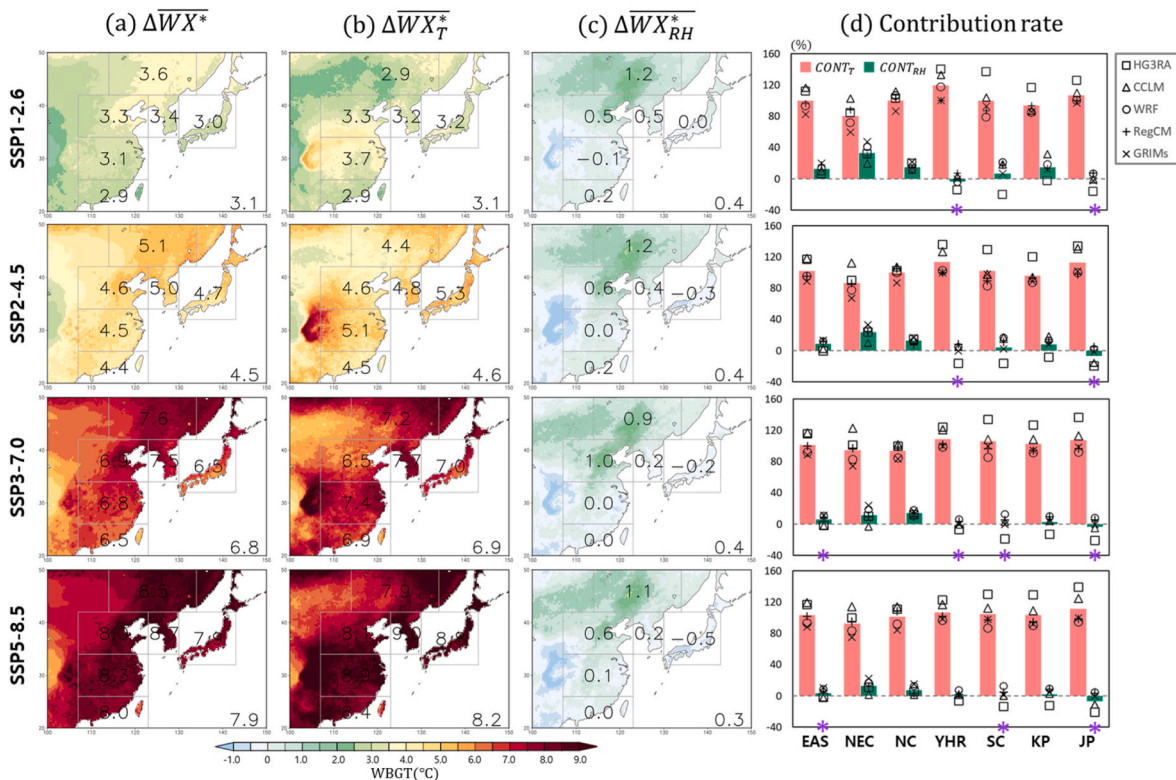

Fig. 4. Spatial distributions of (a) future changes in $\overline{WX^*}$, (b) changes in $\overline{WX^*}$ due to T, and (c) changes in $\overline{WX^*}$ due to RH from five RCMs MME, and (d) contribution rate (%) of T and RH to changes in $\overline{WX^*}$ for EAS and six sub-regions in the late 21st century. (* denote weak consistency among the RCMs, indicating that 3 or fewer models out of 5 RCMs showed a different trend from the MME).

the overall increase of its positive contribution and the weakening of its negative contribution. In the NEC region, where the positive contribution of RH is most pronounced, the contribution is +2.9–14.3% in the summer average state in four SSP scenarios, but increases to +12.9–33.3% in the hottest summer days. The YHR region, where RH decreases, shows a negative contribution of −6.3 to −4.7% in the summer average state, but the negative contribution is reduced to −3.2 to 0% in the hottest summer days. Among five RCMs, HadGEM3-RA simulates the highest temperature increase in most regions, showing a high temperature contribution compared to other models and a low relative humidity contribution (Fig. S6b). GRIMs, on the other hand,

project a significant increase in RH in the NEC and NC regions compared to other models, resulting in a greater impact of RH on hottest summer days in these regions. While the model spread is larger compared to $\overline{WX}$, the individual characteristics of each RCM remain similar.

3.2. Sub-regional changes in extreme heat stress days (EHDs)

To explore the future changes in the spatiotemporal characteristics of extreme heat stress, the frequency, intensity, spatial extent, magnitude, and duration of extreme heat stress days (EHDs, see section 2.4) are projected for each sub-region. EHDs by sub-region occur annually an
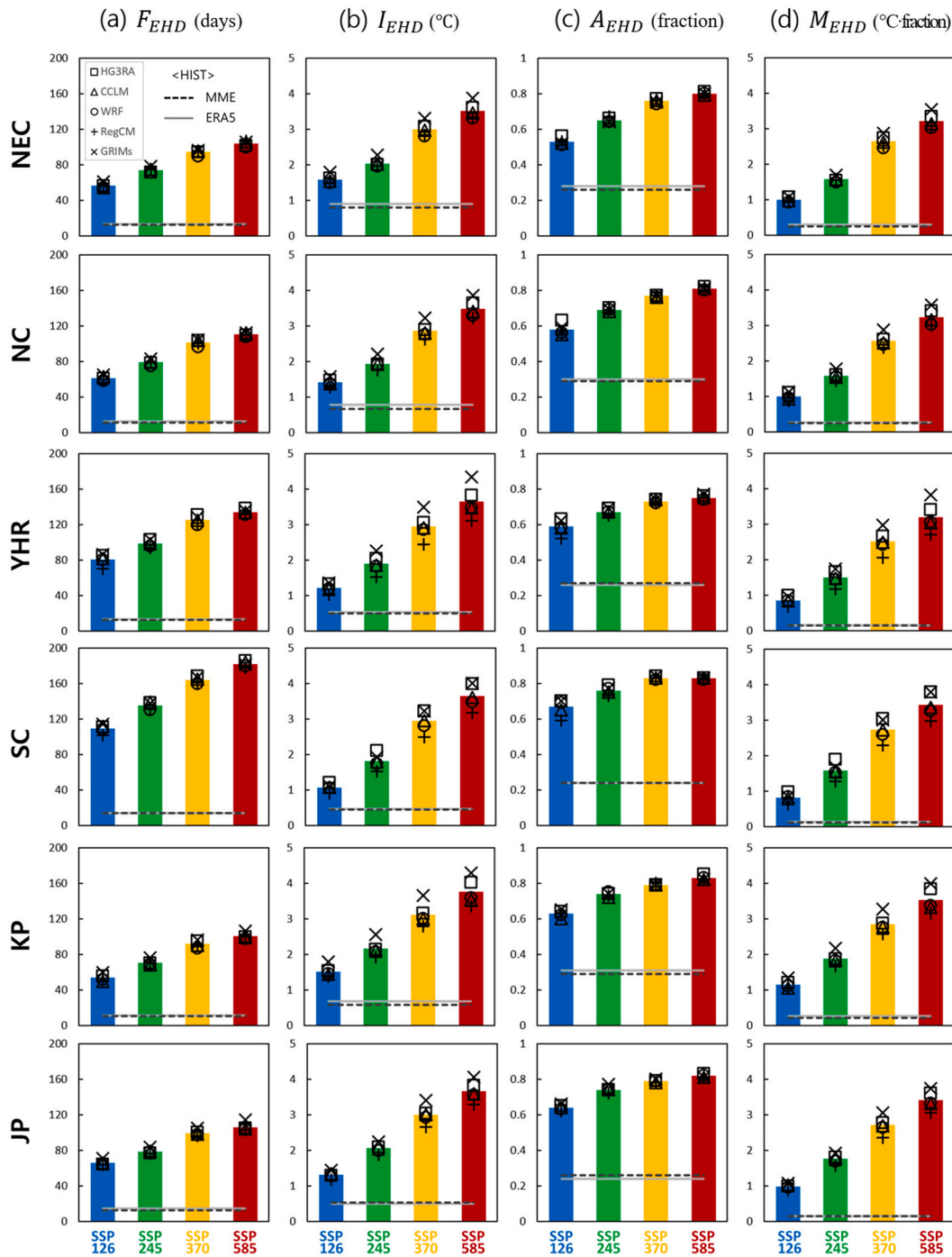

Fig. 5. Future projections for (a) frequency, (b) intensity, (c) spatial extent, and (d) magnitude of EHDs in the late 21st century for six sub-regions. Bars represent the MME results and marks depict each RCM results. Gray horizontal solid line and black dashed line indicate the ERA5 and MME values for the current period, respectively.

average of 12.5 days (six sub-region averages) in the current climate (Fig. 5a). EHDs occur the most frequently in the SC region (14.0 days), and the least frequently in the KP region (10.8 days). The SC is the area with the highest relative humidity among the five sub-regions, and even with the same temperature increase, the rise in WBGT is more pronounced compared to other regions. Moreover, due to the high relative humidity, the seasonal cycle amplitude of temperature is lower in this region (Fig. S7). As a result, it is expected that even small increases in temperature would lead to numerous days reaching the threshold of extreme. This suggests that in the SC region, the frequency of EHDs is expected to increase significantly compared to other sub-regions. This aligns with the findings of Park et al. (2021), which indicate that in the low-latitude regions of East Asia, there is a greater increase in the number of hot days as the summer seasons lengthen. The higher the emission scenario, the greater the frequency of occurrence. In the SSP5-8.5 scenario, EHDs are expected to occur 10 times more frequently in all sub-regions in the late 21st century than present. In particular, the SC region is expected to experience the largest increase in EHDs frequency, with 109.4 days in SSP1-2.6 scenario and 181.4 days in SSP5-8.5 scenario.

The intensity of EHDs (I_{EHD}) is from 0.5 to 0.8 °C in the current climate (Fig. 5b). In the late 21st century, the intensity is expected to increase in all sub-regions by 1.1–1.6 °C in the low-emission scenario (SSP1-2.6) and by 3.5–3.8 °C in the high-emission scenario (SSP5-8.5). The difference in intensity projections among five RCMs is larger than that in frequency. In all sub-regions excluding SC, GRIMs exhibits a higher intensity of extreme heat stress, while RegCM4 simulates relatively low intensity, consistent with the projections in hottest summer days ($\overline{WX}^*$, Fig. S5). In the SC region, HadGEM3-RA simulates a larger increase in temperature for the low-emission scenario, while both HadGEM3-RA and GRIMs simulate a higher temperature for the high-emission scenario. Since both models project stronger increases in summer mean WX ($\overline{WX}$) than other models (Fig. S3), our results support that models simulating larger changes in mean WX also project larger increases in extreme WX.

The spatial extent of EHDs (A_{EHD}) is currently 25–30% in each sub-region (Fig. 5c). However, in the late 21st century, the spatial extent of extreme heat stress increases to 50–60% in low-emission scenario and 70–80% in high-emission scenario, indicating that a larger part of East Asia is affected by extreme heat stress events. As the emission gets higher, the spatial extent of EHDs expands more with good inter-RCM agreement. As both intensity and spatial extent EHDs increases, the
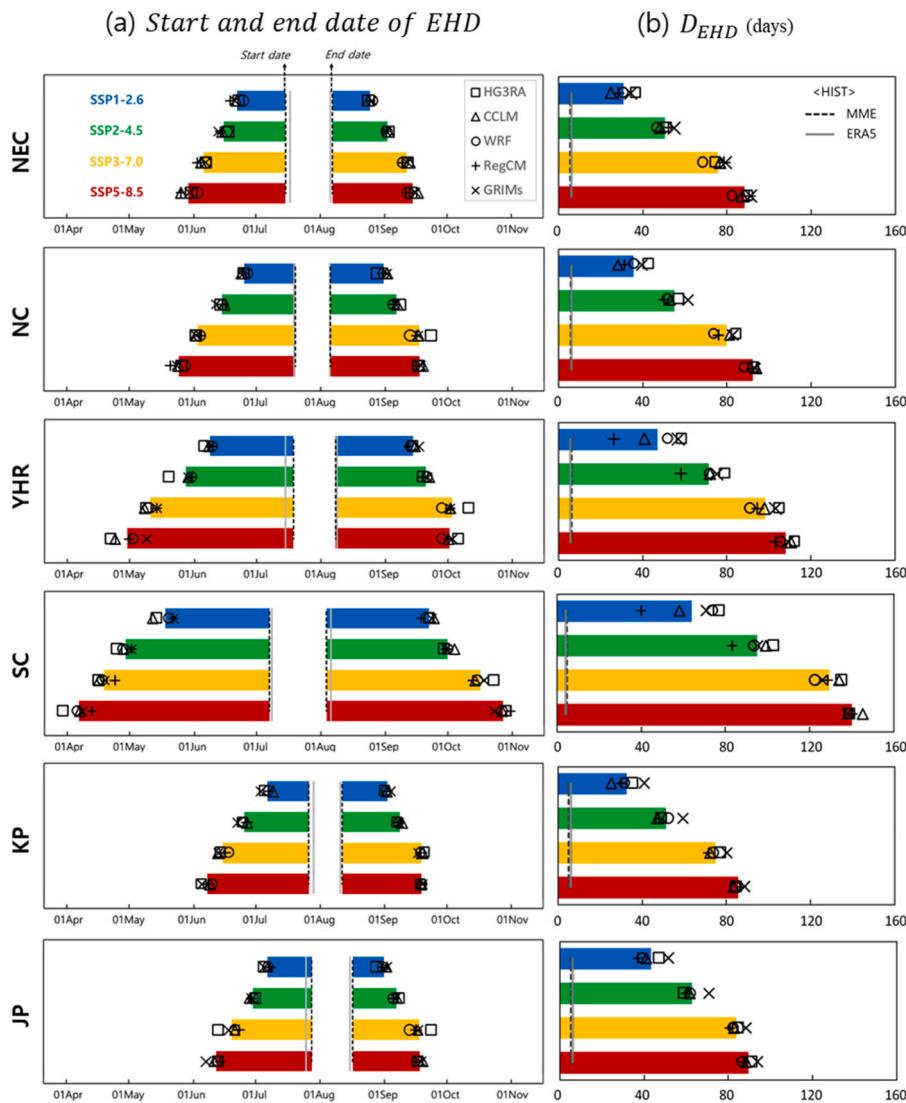

Fig. 6. Future projections for (a) start and end date and (b) maximum duration of EHDs for six sub-regions in the late 21st century. EHDs lasting at least three days are only considered. Bars represent the MME results and marks depict each RCM results. Gray vertical solid line and black dashed line indicate the ERA5 and MME values for the current period, respectively.

magnitude (M_{EHD}) that simultaneously considers them increase substantially (Fig. 5d). Currently, the M_{EHDs} range from 0.1 to 0.2 °C•fraction in all sub-regions, but this is expected to strengthen to 3.2–3.5 °C•fraction under the high-emission scenario (SSP5-8.5) in the late 21st century. As a result, such severe heat stress may occur much more frequently in the late 21st century. Similar to the intensity results, GRIMs generally show higher magnitude of EHDs whereas RegCM4 simulates relatively low magnitude in most regions.

We analyzed the temporal occurrence characteristics of EHDs for each sub-region. In all sub-regions, the start date of EHDs (which lasts at least three consecutive days) is expected to be advanced, and the end date of EHDs is expected to be delayed in the future (Fig. 6). The higher the emission scenario, the longer the duration of EHDs (from the start date to the end date). In the SSP5-8.5 scenario, the start date of EHDs is advanced by 52 days (JP) to 86 days (SC) compared to the present, and the end date is delayed by 39 days (KP) to 79 days (SC). On average, the possible occurrence period of EHDs is 120 days longer, and the expansion of the possible occurrence period of EHDs in YHR and SC located at low latitude is particularly strong. The SC region shows the earliest start date and the latest end date of EHDs among six regions. According to the SSP5-8.5, EHDs in the SC region on average begin to occur in early April and are expected to appear by the end of October. The changes under the SSP scenarios are more pronounced at the start date than at the end date. Compared to the SSP5-8.5, the SSP3-7.0 scenario shows that the start date is advanced but the end date remains unchanged in many regions (NC, YHR, KP and JP). When examining the future projections of WX and T for the starting period of EHD in May–June compared to the ending period in September–October (Fig. S8), it becomes evident that the WX and T in late spring and early summer are significantly higher than in early autumn. This suggests that in the future, these periods will reach the threshold of extreme WBGT (WX_{95p}) earlier. Consequently, the advancement of the starting date appears to undergo a more distinct change compared to the delay in the ending date.

EHDs occur on a regional scale while maintaining spatial continuity (over 30% overlap) and lasting an average of five to six days. In the SSP5-8.5 scenario, the maximum duration of EHDs (D_{EHD}) in all sub-regions will be on average more than 80 days, meaning that the extreme heat stress events continue over most of the summer. As in start and end date projections, YHR and SC region have longer maximum duration than other regions. In particular, southern China is expected to have an average maximum duration of more than 140 days in the late 21st century, lasting more than four months once EHDs occur. In the East Asia, the lowest latitude area, SC, exhibits the most pronounced changes in the characteristics of extreme heat stress, including frequency, duration, and start/end date. This is in accord with the findings of Chen et al. (2020), which indicate that globally, the intensification of heat stress waves is most prominent in tropical and subtropical regions. In particular, regions with high population density and urbanization, such as the Yangtze River basin, and southern China, which have experienced severe heat stress during the observational period (Luo and Lau, 2019), are expected to continue to experience a pronounced increase in extreme heat stress in the future.

The results by RCMs reveal a larger spread in the low emission scenarios. This difference is particularly noticeable in the YHR and SC regions, located in the lower latitudes of China, where HadGEM3-RA simulates the longest duration of EHDs and RegCM4 simulates the smallest increase in duration. As analyzed above, GRIMs simulates the enhancement of extreme heat stress due to humidity change, and the relatively long duration of extreme heat stress events in these regions might be influenced by humidity.

4. Summary and conclusions

This study examines the future changes in spatiotemporal characteristics of extreme heat stress in East Asia and its sub-regions based on the WBGT index using CORDEX East Asia multi-RCM simulations performed under four SSP (SSP1-2.6, 2–4.5, 3–7.0, 5–8.5) scenarios. We utilized daily maximum WBGT (WX) which were estimated from 3-hourly temperature and humidity data and then biased corrected using a Quantile Delta Mapping method. Results show that East Asia will experience increases in summer mean WX by 3.2 °C (SSP1-2.6) to 7.6 °C (SSP5-8.5) in the late 21st century (2081–2100) with respect to the current period (1979–2014). HadGEM3-RA and GRIMs simulate a larger increase in WX in most regions compared to the other models, with particularly significant increases simulated by HadGEM3-RA in southern China. The summer mean WX changes are mostly driven by temperature changes but, depending on regions and scenarios, changes in relative humidity are found to either exacerbate or alleviate WX changes. The summer mean relative humidity is projected to increase in northern China, resulting in enhanced WX increases by up to 14% (SSP1-2.6), while relative humidity will decrease in the Yangtze River basin and Japan, offsetting the warming-driven WX increases by up to −6% (SSP2-4.5). Notably, the contribution of relative humidity to heat stress is more pronounced during hottest summer days (top 5%) than during average summer conditions. In the SSP1-2.6 scenario, it was found that the increase in relative humidity in northern China enhanced the WX increase on hottest summer days by about 33%. Among the five RCMs, HadGEM3-RA shows a larger temperature increase than other models, indicating a stronger contribution of temperature to the future heat stress changes in most regions. Meanwhile, GRIMs exhibits a larger increase in relative humidity in northern China than other RCMs, enhancing the heat stress increases.

To understand the spatiotemporal characteristics of extreme heat stress at the regional scale, we analyzed the extreme heat stress days (EHDs) defined as days when WX exceeds its 95th percentile threshold over larger than 10% of the area for each sub-region. According to the high-emission scenario, it is expected that EHDs will occur 10 times more frequently across East Asia in the late 21st century than at present. As the high-emission scenario progresses, the intensity of extreme heat stress will gradually increase up to 3.5–3.8 °C, and the spatial extent will expand up to 80%, as well reflected by the magnitude index. Moreover, in the late 21st century, it is predicted that extreme heat stress lasting 80 days or longer will occur in all sub-regions, and most East Asia regions will be affected by severe heat stress all throughout the summer season. In particular, southern China is projected to experience extreme heat stress events lasting more than four months, which will exert huge socioeconomic impacts. Our projection results emphasize the urgent need to reduce greenhouse gas emissions to minimize the effects of severe heat stress on all East Asian land areas and also to take measures to adapt to the upcoming unavoidable climate conditions.

In this study, we used a simplified WBGT index based on temperature and relative humidity. While this approach offers the advantage of simplicity in calculations, it neglects the contributions of solar radiation and wind components in assessing heat stress changes, which may lead to potential overestimations. However, we defined extreme heat stress based on percentile-based relative criteria, aiming to remove the potential impacts of overestimation as much as possible. Additionally, when assessing the contributions of temperature and humidity to heat stress changes, there are limitations in precisely evaluating the effects of their interaction. It has been observed that the interaction between temperature and humidity alleviates temperature-driven heat stress increases in all scenarios (Fig. S9). This effect varies by region, with a more pronounced effect in dry inland areas, such as the YHR region. This compensatory effect due to the interaction between temperature and relative humidity increases as emissions scenarios become more severe. Nevertheless, despite this interaction effect, it is projected that the entire East Asia region will experience severe heat stress in the late 21st century due to increase in temperatures.

Author statement

Yujin Kim: Methodology, Formal analysis, Writing- Original draft

preparation. **Seung-Ki Min**: Conceptualization, Supervision, Writing-Original draft preparation. **Yeon-Hee Kim**: Validation, Writing-Reviewing and Editing. **Eun-Soon Im**: Data curation, Validation, Writing- Reviewing and Editing. **Dong-Hyun Cha**: Data curation. **Joong-Bae Ahn**: Data curation. **Eun-Chul Chang**: Data curation. **Young-Hwa Byun**: Data curation. **Youngeun Choi**: Methodology.

Declaration of competing interest

The authors declare that they have no known competing financial interests or personal relationships that could have appeared to influence the work reported in this paper.

Data availability

Data will be made available on request.

Acknowledgments

Appendix A. Supplementary data

Supplementary data to this article can be found online at https://doi.org/10.1016/j.wace.2023.100618.

References

ACSM, 1984. Prevention of thermal injuries during distance running: position stand. Med. J. Aust. 141, 876–879.

Chen, X., Li, N., Liu, J., Zhang, Z., Liu, Y., Huang, C., 2020. Changes in global and regional characteristics of heat stress waves in the 21st century. Earth's Future 8 (11), e2020EF001636.

Chindapol, S., Blair, J., Osmond, P., Prasad, D., 2017. A suitable thermal stress index for the elderly in summer tropical climates. Procedia Eng. 180, 932–943.

Coffel, E.D., Horton, R.M., De Sherbinin, A., 2017. Temperature and humidity based projections of a rapid rise in global heat stress exposure during the 21st century. Environ. Res. Lett. 13 (1), 014001.

Fischer, E.M., Oleson, K.W., Lawrence, D.M., 2012. Contrasting urban and rural heat stress responses to climate change. Geophys. Res. Lett. 39 (3).

Fischer, E.M., Knutti, R., 2013. Robust projections of combined humidity and temperature extremes. Nat. Clim. Change 3 (2), 126–130.

Ha, K.J., Seo, Y.W., Yeo, J.H., Timmermann, A., Chung, E.S., Franzke, C.L., Chan, J.C.L., Yeh, S.W., Ting, M., 2022. Dynamics and characteristics of dry and moist heatwaves over East Asia. npj Clim. Atmospher. Sci. 5 (1), 49.

Hersbach, H., Bell, B., Berrisford, P., Biavati, G., Horányi, A., Muñoz Sabater, J., Nicolas, J., Peubey, C., Radu, R., Rozum, I., Schepers, D., Simmons, A., Soci, C., Dee, D., Thépaut, J.-N., 2023. ERA5 Hourly Data on Single Levels from 1940 to Present, Copernicus Climate Change Service (C3S) Climate Data Store (CDS). https://doi.org/10.24381/cds.adbb2d47.

Im, E.-S., Choi, Y.-W., Ahn, J.-B., 2017. Worsening of heat stress due to global warming in South Korea based on multi-RCM ensemble projections. J. Geophys. Res. Atmos. 122 (21), 11444–11461. https://doi.org/10.1002/2017JD026731.

Ioannou, L.G., Tsoutsoubi, L., Mantzios, K., Vliora, M., Nintou, E., Piil, J.F., Notley, S.R., Dinas, P.C., Gourzoulidis, G.A., Havenith, G., Brearley, M., Mekjavic, I.B., Kenny, G.P., Nybo, L., Flouris, A.D., 2022. Indicators to assess physiological heat strain–Part 3: multi-country field evaluation and consensus recommendations. Temperature 9 (3), 274–291.

IPCC, 2021. Summary for Policymakers. In: Masson Delmotte, V., Zhai, P., Pirani, A., Connors, S.L., Pean, C., Berger, S., Caud, N., Chen, Y., Goldfarb, L., Gomis, M.I., Huang, M., Leitzell, K., Lonnoy, E., Matthews, J.B.R., Maycock, T.K., Waterfield, T., Yelekçi, O., Yu, R., Zhou, B. (Eds.), Climate Change 2021: The Physical Science Basis. Contribution of Working Group I to the Sixth Assessment Report of the Intergovernmental Panel on Climate Change. Cambridge University Press, Cambridge, United Kingdom and New York, NY, USA, pp. 3–32. https://doi.org/10.1017/9781009157896.001.

Juzbašić, A., Ahn, J.B., Cha, D.H., Chang, E.C., Min, S.K., 2022. Changes in heat stress considering temperature, humidity, and wind over East Asia under RCP8. 5 and SSP5-8.5 scenarios. Int. J. Climatol. 42 (12), 6579–6595.

Keellings, D., Moradkhani, H., 2020. Spatiotemporal evolution of heat wave severity and coverage across the United States. Geophys. Res. Lett. 47 (9), e2020GL087097.

Knutson, T.R., Ploshay, J.J., 2016. Detection of anthropogenic influence on a summertime heat stress index. Climatic Change 138 (1–2), 25–39.

Kim, Y.H., Ahn, J.B., Suh, M.S., Cha, D.H., Chang, E.C., Min, S.K., Byun, Y.H., Kim, J.U., 2023. Future changes in extreme heatwaves in terms of intensity and duration over the CORDEX-East Asia Phase Two domain using multi-GCM and multi-RCM chains. Environ. Res. Lett. 18 (3), 034007.

Kim, Y., Choi, Y., Min, S.K., 2022. Future changes in heat wave characteristics and their impacts on the electricity demand in South Korea. Weather Clim. Extrem. 37, 100485.

Kong, Q., Huber, M., 2022. Explicit calculations of wet-bulb globe temperature compared with approximations and why it matters for labor productivity. Earth's Future 10 (3), e2021EF002334.

Lee, D., Min, S.K., Ahn, J.B., Cha, D.H., Shin, S.W., Chang, E.C., Suh, M.S., Byun, Y.H., Kim, J.U., 2023. Uncertainty analysis of future summer monsoon duration and area over East Asia using a multi-GCM/multi-RCM ensemble. Environ. Res. Lett. https://doi.org/10.1088/1748-9326/acd208.

Lee, S.M., Min, S.K., 2018. Heat stress changes over East Asia under 1.5 and 2.0 C global warming targets. J. Clim. 31 (7), 2819–2831.

Li, Y., Li, C., Luo, S., He, J., Cheng, Y., Jin, Y., 2017. Impacts of extremely high temperature and heatwave on heatstroke in Chongqing, China. Environ. Sci. Pollut. Control Ser. 24, 8534–8540.

Liu, X., Tang, Q., Zhang, X., Sun, S., 2018. Projected changes in extreme high temperature and heat stress in China. J. Meteorol. Res. 32 (3), 351–366.

Luo, M., Lau, N.C., 2019. Characteristics of summer heat stress in China during 1979–2014: climatology and long-term trends. Clim. Dynam. 53 (9–10), 5375–5388.

Luo, M., Lau, N.C., Liu, Z., Wu, S., Wang, X., 2022. An observational investigation of spatiotemporally contiguous heatwaves in China from a 3D perspective. Geophys. Res. Lett. 49 (6), e2022GL097714.

Lyon, B., Barnston, A.G., Coffel, E., Horton, R.M., 2019. Projected increase in the spatial extent of contiguous US summer heat waves and associated attributes. Environ. Res. Lett. 14 (11), 114029.

Matthews, T.K., Wilby, R.L., Murphy, C., 2017. Communicating the deadly consequences of global warming for human heat stress. Proc. Natl. Acad. Sci. USA 114 (15), 3861–3866.

Mora, C., Dousset, B., Caldwell, I.R., Powell, F.E., Geronimo, R.C., Bielecki, C.R., Counsell, C.W.W., Dietrich, B.S., Johnston, E.T., Louis, L.V., Lucas, M.P., Mckenzie, M.M, Shea, A.G., Tseng, H., Giambelluca, T.W., Leon, L.R., Hawkins, E., Trauernicht, C., 2017. Global risk of deadly heat. Nature Climate Change 7 (7), 501–506.

Park, B.J., Min, S.K., Weller, E., 2021. Lengthening of summer season over the Northern Hemisphere under 1.5 C and 2.0 C global warming. Environ. Res. Lett. 17 (1), 014012.

Park, C., Shin, S.W., Cha, D.H., Suh, M.S., Hong, S.Y., Ahn, J.B., Min, S.K., Byun, Y.H., 2022. Future projections of precipitation using bias–corrected high–resolution regional climate models for sub–regions with homogeneous characteristics in South Korea. Asia-Pacific J. Atmosph. Sci. 58, 715–727.

Peng, J.B., Cholaw, B., 2011. The definition and classification of extensive and persistent extreme cold events in China. Atmos. Oceanogr. Sci. Libr. 4 (5), 281–286.

Qiu, L., Im, E.-S., Min, S.-K., Kim, Y.-H., Cha, D.-H., Shin, S.-W., Ahn, J.-B., Chang, E.-C., Byun, Y.-H., 2023. Direct and indirect application of univariate and multivariate bias corrections on heat-stress indices based on multi regional-climate-model simulations. Earth Syst. Dynam. 14 (2), 507–517.

Ren, F., Cui, D., Gong, Z., Wang, Y., Zou, X., Li, Y., Wang, S., Wang, X., 2012. An objective identification technique for regional extreme events. J. Clim. 25 (20), 7015–7027.

Schwingshackl, C., Sillmann, J., Vicedo-Cabrera, A.M., Sandstad, M., Aunan, K., 2021. Heat stress indicators in CMIP6: estimating future trends and exceedances of impact-relevant thresholds. Earth's Future 9 (3), e2020EF001885.

Simpson, C.H., Brousse, O., Ebi, K.L., Heaviside, C., 2023. Commonly used indices disagree about the effect of moisture on heat stress. npj Clim. Atmospher. Sci. 6 (1), 78.

Takakura, J.Y., Fujimori, S., Takahashi, K., Hijioka, Y., Honda, Y., 2019. Site-specific hourly resolution wet bulb globe temperature reconstruction from gridded daily resolution climate variables for planning climate change adaptation measures. Int. J. Biometeorol. 63, 787–800.

Wang, Y., Ren, F., Zhang, X., 2014. Spatial and temporal variations of regional high temperature events in China. Int. J. Climatol. 34 (10), 3054–3065.

Wang, P., Tang, J., Wang, S., Dong, X., Fang, J., 2018. Regional heatwaves in China: a cluster analysis. Clim. Dynam. 50, 1901–1917.

Wang, P., Hui, P., Xue, D., Tang, J., 2019. Future projection of heat waves over China under global warming within the CORDEX-EA-II project. Clim. Dynam. 53, 957–973.

Willett, K.M., Sherwood, S., 2012. Exceedance of heat index thresholds for 15 regions under a warming climate using the wet-bulb globe temperature. Int. J. Climatol. 32 (2), 161–177.

Yaglou, C.P., Minard, D., 1957. Control of heat casualties at military training centers. Amer. Med. Assoc. Arch. Ind. Health 16, 302–316.

Yoon, D., Cha, D.H., Lee, M.I., Min, K.H., Kim, J., Jun, S.Y., Choi, Y., 2020. Recent changes in heatwave characteristics over Korea. Clim. Dynam. 55, 1685–1696.

Zamanian, Z., Sedaghat, Z., Hemehrezaee, M., Khajehnasiri, F., 2017. Evaluation of environmental heat stress on physiological parameters. J. Environ. Health Sci. Eng. 15, 1–8.